Available online at www.sciencedirect.com

SciVerse ScienceDirect

Procedia CIRP 6 (2013) 492 – 497

www.elsevier.com/locate/procedia

The Seventeenth CIRP Conference on Electro Physical and Chemical Machining (ISEM)

Influence of weld bead geometry on thermal deformation in laser micro-welding

S. Matsuoka[a], Y. Okamoto[a,*], A. Okada[a]

[a]*Okayama University, 3-1-1 Tsushimanaka, Kita-ku, Okayama 700-8530, Japan*

* Corresponding author. Tel.: +81-86-251-8039 ; fax: +81-86-251-8266 .*E-mail address*: okamoto@mech.okayama-u.ac.jp.

Abstract

In this study, the thermal deformation of thin stainless steel sheet was investigated in the bead-on-plate welding by using a single-mode fiber laser with a Galvano scanning system. The numerical simulation was developed to calculate the temperature and stress fields, and its deformation characteristics were discussed. It was suggested that the specimen firstly deformed downward in the same direction of laser irradiation, and then deformed in the reversed direction after laser scanning. The final deformation angle in the negative direction, which is concave shape from the view direction of laser irradiation, was generated under the welding mode of conduction and quasi-penetration for 50 µm thickness sheet. On the other hand, the positive angle of final deformation angle was obtained under full-penetration welding mode, and the extreme small distortion could be achieved by the proper weld bead geometry in micro-welding of thin sheet. It was also confirmed that the similar weld bead geometry was resulted in both quasi-penetration and full-penetration welding mode for 20 µm thickness sheet, but the final deformation angle tendency was different in 50 µm and 20 µm specimen thickness. It was clarified that the welding deformation was influenced not only by weld bead geometry but also by specimen thickness.

Keywords: Micro-welding; Thermal deformation; Single-mode fiber laser; High-speed scanning.

1. Introduction

Recently, the micro-joining of small components has been strongly required, since the electronic devices have become smaller, thinner and lighter in the industrial applications for the higher functionality and the lower cost. For these parts, austenitic stainless steel SUS304 with high weldability has been widely used. However, the distortion often occurs due to the heat input in welding process. The laser micro-welding is one of attractive methods in the micro-joining technique, since the high spatial and temporal control could be expected by the high quality laser beam [1]-[2]. In addition, there is the advantage as non-contact processing, in which the reaction force does not be loaded from a workpiece. Thus, a high-precision joint can be expected even at the side wall of narrow cavity and for the combination of dissimilar materials, which were difficult to weld by the conventional welding method. In general, it is important to control the heat input to the specimen in micro-welding of thin steel sheet, since burn-through, welding deformation and the weld bead geometry have an influence on the quality of weld joint [3]-[4].

The weld bead geometry is determined by laser power, scanning velocity and beam spot diameter, and its geometry is very essential to evaluate the weld joint. It is considered that precision micro-joining with small heat affected zone would be performed by the laser micro-welding, but the welding deformation could not be ignored. The bending and deformation in the laser forming process had been reported [5], but the welding deformation of thin stainless steel sheet by the laser micro-welding has not been clarified yet. Therefore, it is important to understand the relationship between the welding deformation and the weld bead geometry in order to accomplish the precision weld joint for the micro-joining of thin sheet.

doi:10.1016/j.procir.2013.03.054

In this study, the thermal deformation of thin stainless steel sheet in laser micro-welding using a single-mode CW fiber laser with a Galvano scanning system was experimentally investigated, and the distributions of temperature and stress were discussed to clarify the thermal deformation in micro-welding by the numerical calculation.

2. Experimental procedures

Figure 1 shows the schematic diagram of experimental setup. In this study, single-mode CW Yb fiber laser of 1090 nm in wavelength was used as a laser source. The laser beam was delivered by an optical fiber and focused by a telecentric type fθ lens of 100 mm in focal length. The laser scanning was carried out by Galvano scanner to achieve the high-speed beam scanning. The expander was installed between the isolator and the bending mirror to decrease the spot diameter of laser beam. The bead-on-plate welding on the austenitic stainless steel SUS304 of 20 and 50 μm in thickness was carried out in shielding gas of nitrogen under a constant supplying pressure 100 kPa. In order to evaluate the welding deformation, the deformation amounts were measured by a laser displacement sensor (LDS).

Figure 2 shows the schematic diagram of deformation measurement setup. The clamping plate with an opening slot of 2 mm was used to ensure the straightness of specimen sheets. Therefore, the deformation measurement was set to 2 mm width and 1 mm length. The clamping plate was also designed with tighten screws to hold the specimen down to the supporting plate. Each line was divided by 25 μm distance and 80 points in total were measured. The deformation value of specimen was defined as the difference of measurement values before and after the laser irradiation experiment.

In this study, the welding deformation is evaluated in deformation angle of specimen as shown in Fig. 3. The deformation angle for individual point *i* is calculated from the measurement of the displacement in the *z*-direction over the length from specimen edge as expressed in equation. The positive angle is defined as the deformation towards the laser beam irradiation direction, while the negative angle is the deformation downwards against the laser beam irradiation direction.

3. Thermo-mechanical analysis method and conditions by finite element method

Figure 4 shows the dimension of geometry model with 1 mm in length, 2 mm in width and 50 μm in thickness. The gaussian distribution of laser energy was used as a heat source, which is considered the summation of surface heat source on the top surface and volume heat source along the thickness direction.The clamping of sheet at both ends was used as the boundary condition in structural analysis. The displacement of specimen was zero at the end of sheet. The analysis

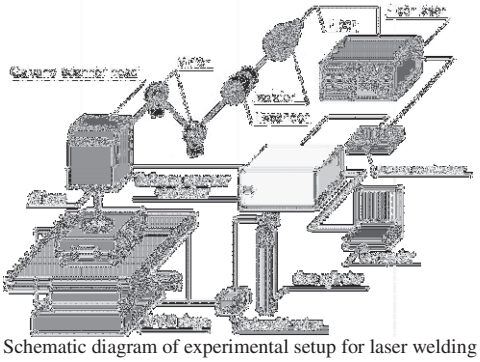

Fig. 1. Schematic diagram of experimental setup for laser welding

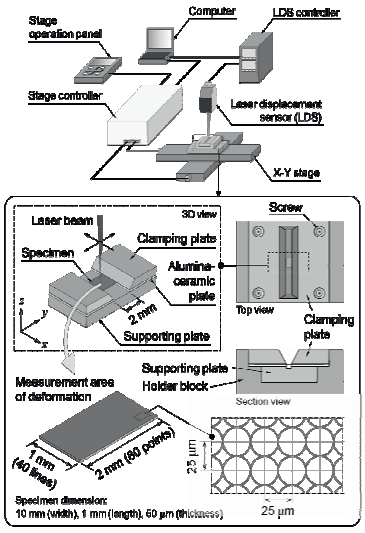

Fig. 2. Schematic diagram of deformation measurement

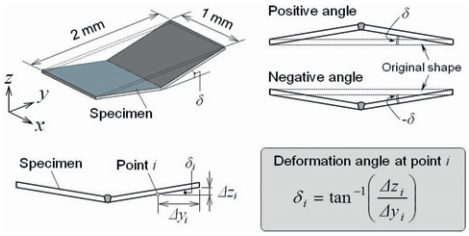

Fig. 3. Definition of deformation angle

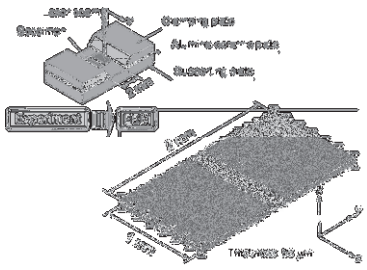

Fig.4. Boundary condition in mechanical analysis

condition was set at laser power 50 W, scanning velocity 1 m/s and spot diameter 35 μm for 50 μm specimen thickness. The general finite element program 'ANSYS Rev. 14.0' was used for the three-dimensional finite element analysis.

The temperature dependent thermophysical properties were used as shown in Figs. 5 (a) and (b), and the temperature dependent mechanical properties were also taken from references [6]-[7]. Since it was reported that there was little influence on the thermal stress by the phase change, the effect of phase change on the thermal stress was not considered in this analysis [8].

4. Numerical simulation results and discussion

Figure 6 shows the cross-sectional views of weld bead obtained by experiment and numerical simulation under the same irradiation condition. The temperature distribution of bead geometry shows the highest temperature in analysis result, and its isothermal shape of melting point agrees well with molten zone in experiment. The temperature, stress, deformation fields were evaluated by this simulation result.

Figure 7 shows the longitudinal stress fields and temperature distributions at the center of scanning line, where the laser beam is located at 500 μm from the edge of specimen (Point A at top surface, Point B at the bottom surface). It can be clearly seen that the point A rapidly reaches the higher compressive stress because the expansion of the molten pool is restrained by the surrounding material. At this time, the point B shows the tensile stress, because of the restriction of the surrounding material. During the cooling period, the compressive stress rapidly decreases due to the rapid cooling and change to the tensile stress due to the contraction of the material at the point A. On the other hand, the compressive stress is generated at the point B to balance the tensile stress at the top surface of point A. Therefore, the final deformation shape of specimen after the cooling period is affected by the difference of magnitude stress between both surfaces.

Figure 8 (a) shows the longitudinal residual stress distribution (σ_{xx}). It can be observed that the residual tensile stress was generated at the center of weld line and it was balanced with compressive stress at base material to maintain the original length significantly during cooling. The longitudinal tensile stress in the molten zone was higher than the longitudinal compressive stress in the base material and the stress gradient within the molten zone is large by high temperature gradient at this region. On the other hand, it was considered that the transverse residual stress distribution (σ_{yy}) was influenced on the angular distortion in Fig. 8 (b). It can be noticed that the high residual tensile stress was generated around the weld line and the compressive stress was generated at the both of specimen edges along the width direction. The transverse residual stress was much smaller than the longitudinal stress, and reached its peak value close to the molten zone or HAZ, and gradually reduces toward to the edge of the specimen.

Figure 9 shows the displacement evaluated at the bottom surface of specimen along the width and scanning directions. The displacements are magnified in these figures to make them clearly visible, and the

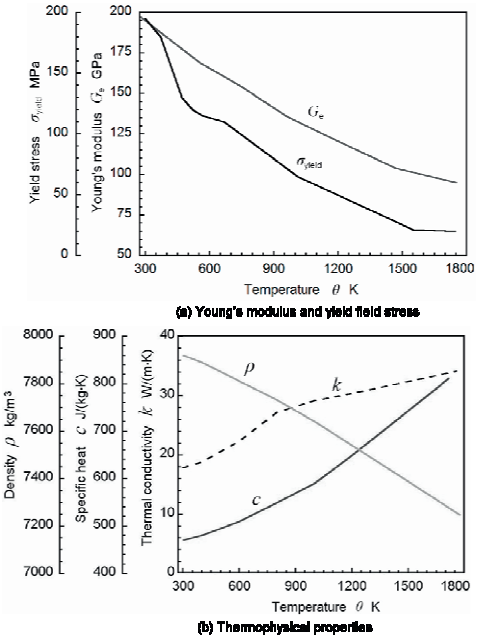

Fig.5. (a) Young's modulus and yield field stress; (b) Thermophysical properties

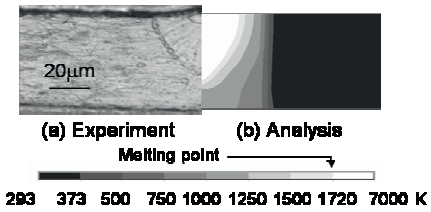

Fig.6. Comparison of weld bead geometry between (a) Experimental and (b) Numerical simulation results

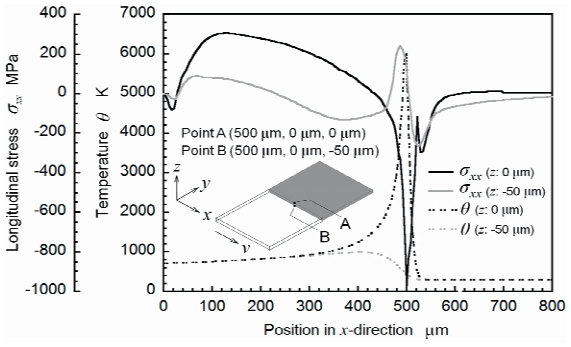

Fig.7 Temperature and longitudinal stress distributions of the top and bottom surface in laser scanning line

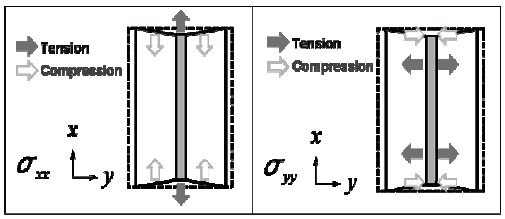

(a) Longitudinal residual stress (b) Transverse residual stress

Fig.8. (a) Longitudinal residual stress distribution; (b) Transverse residual stress distribution

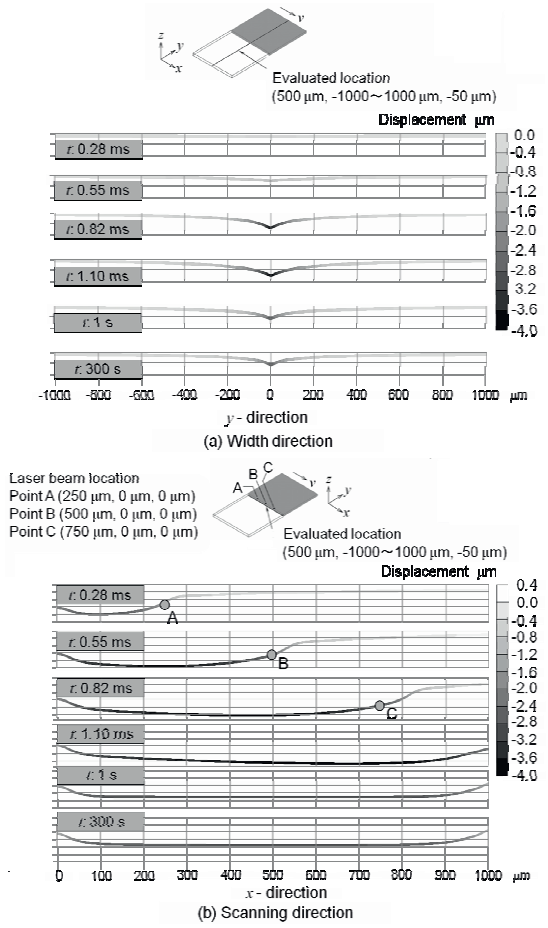

Fig. 9. Displacement of specimen during and after laser irradiation (a) Width direction; (b) Scanning direction

circles on the curves indicate the locations of the laser beam. The angular deformation of specimen shows the tendency to become concave to the laser irradiation side until the end of cooling period. It is shown that the specimen firstly deformed downward in the same direction of laser irradiation. Then it deformed in the reversed direction, but it still remained with the concave shape to the laser irradiation side. In addition, it can be also observed that buckling deformation occurred during irradiation period at displacement along welding direction, which is caused by compressive stress. This phenomenon would become instability of welding deformation. From these results, it was clarified thermal deformation was influenced by change of the stress field generated during the heating and cooling period. It is noticed that the change of stress field also depended on the weld bead geometry, which was varied by the energy density and the power density.

5. Experimental results and discussion

In this experiment, thermal deformation was investigated with changing the energy density and the power density, which was greatly influenced on weld bead geometry. The bead-on-plate experiment was carried out 3 times under the same irradiation condition, and their averages were calculated as deformation angle.

Figure 10 shows the experimental result of measured displacement at the top surface of specimen and deformation angle under the constant scanning velocity 1 m/s and the spot diameter 35 μm. The displacement is the subtraction value between the final displacement after welding and the initial displacement before welding. In terms of weld bead geometry, the weld bead became larger with the increase of laser power, and the deeper weld bead depth as quasi- and full-penetrations were observed under the higher energy and the power density condition. It shows that the large deformation was generated under the low laser power condition. The conduction (P: 30 W) and quasi-penetration (P: 50 W) welding modes induced the final deformation of concave shape to the laser irradiation side. In contrast, the final deformation in full-penetration welding mode (P: 60 W) resulted in a convex shape to the laser irradiation side. As shown in Fig. 9 (d), it was confirmed that the deformation angle also increased with increasing the penetration depth. In addition, this relationship would suggest that the small welding deformation could be achieved with proper control of laser power by obtaining the weld bead depth from 30 to 50 μm for 50 μm thickness sheet.

Figure 11 shows thermal deformation under each laser irradiation conditions in the bead-on-plate welding for 50 μm thickness sheet. This figure summarizes the influence of energy density, which defined as the laser power divided by the scanning velocity and the spot diameter. It can be noticed here that the energy density has directly related to the welding mode and the weld bead geometry. The energy density also contributes significantly on the welding deformation. It was confirmed that thermal deformation was also different depending on the scanning velocity. On the other hand, in full-penetration welding mode, the humping was occurred when the scanning velocity was fast. It was one of the weld defects, and the weld bead has been lifted to the surface from the middle specimen in full-penetration

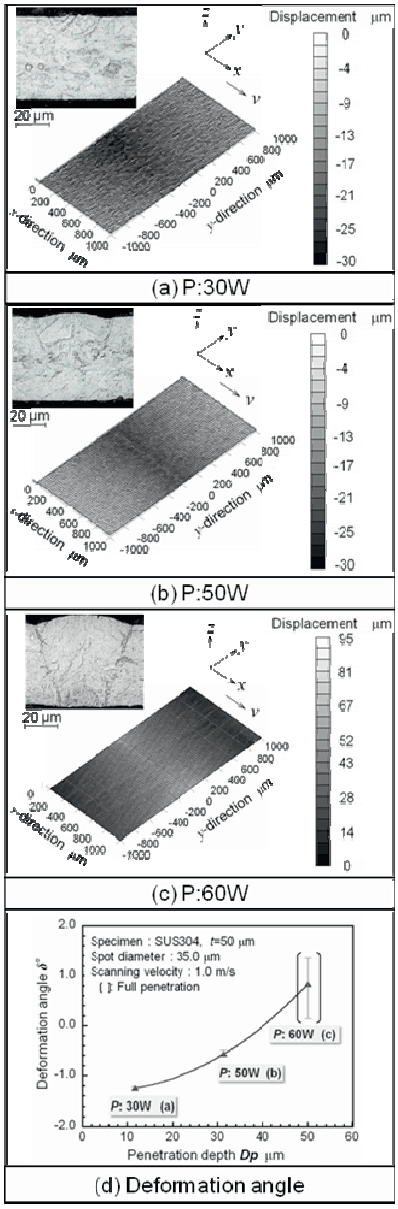

Fig.10. (a)-(c) Weld bead geometry and measured displacement at 30W, 50W and 60 W; (d) relationship between deformation angle and penetration depth (v: 1.0m/s, d:

conditions. In the results of deformation angle in actual experiments, it was clarified that the deformation angle was positive in full-penetration welding mode due to both the shrinkage of width direction related to humping and the expansion of weld bead with the convex curvature on the top surface. Therefore, it can be considered that the control of scanning velocity plays an important role to produce a precision joint.

Figure 12 shows the extreme small deformation for 50 μm thickness sheet in the bead-on-plate welding. As can be seen from the figure, the deformation was

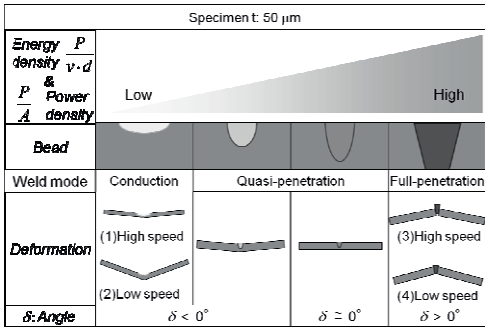

Fig.11. Thermal deformation for 50 μm thickness sheet

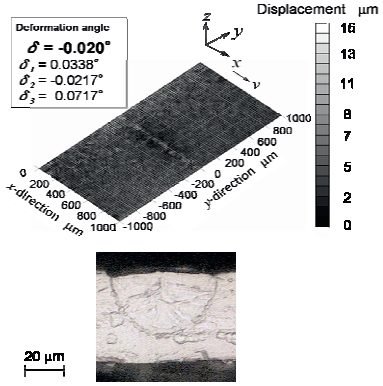

Fig.12. Extreme small deformation (P: 56W, v: 1.0m/s, d: ϕ 35.0μm)

extremely small, and the deformation angle was almost resulted in 0 degree. In the case of 50 W as shown in Fig. 10 (b), the deformation angle was large, and the penetration depth was smaller than 30 μm. On the other hand, the penetration depth was approximately 35 μm for 50 μm thickness of specimen, when the deformation angle was almost 0 degree.

It was clarified that the micro-welding with extreme small distortion could be achieved by the proper weld bead geometry, in which the penetration depth was a little smaller than the thickness of specimen. Thermal contraction was caused by the rapid cooling, and the tensile stress generated in and around the molten zone as residual stress. However, the balance of stress was different by the penetration depth and specimen thickness, and the difference of tensile stress value was occurred between the top and the bottom surface of specimen. The equivalent penetration depth to the thickness of specimen would lead to the minimal distortion, since the tensile stress was balanced at the top and bottom sides of specimen.

In order to investigate the relationship between the welding deformation and the weld bead geometry for other specimen thickness, the welding deformation was evaluated by using 20 μm thickness sheet.

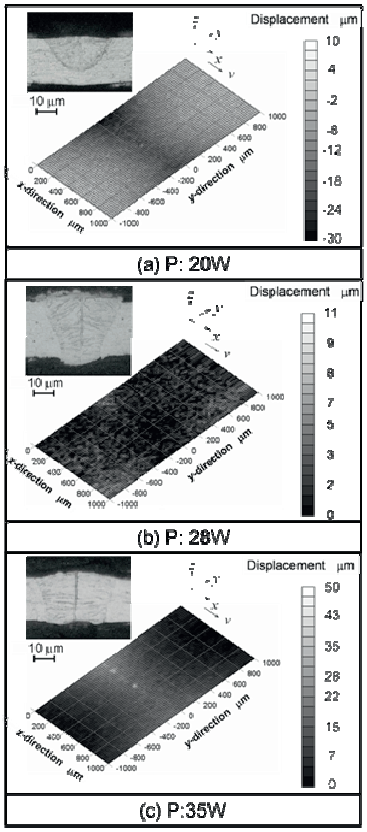

Fig.13. (a)-(c) Weld bead geometry and measured displacement at 20W, 28W and 30 W in the case of 20 μm thickness sheet (v: 1.0m/s, d: ϕ35.0μm)

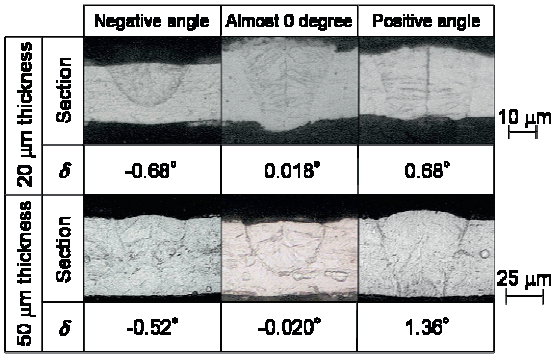

Fig.14. Comparison of deformation angle and weld bead geometry between 50 μm and 20 μm specimen thickness

Figure 13 shows the measured results of final displacement for 20 μm thickness sheet. It was confirmed that the penetration depth increased with increasing the energy density. The final deformation of specimen was also resulted in concave shape in the quasi-penetration. On the other hand, in the full-penetration mode, both the flat shape and the convex shape were obtained as final welding deformation. It was considered that the bead width of 20 μm thickness was wider than that of 50 μm thickness, and it was also different at the top and bottom surface, which would result in the large transverse shrinkage as shown in Fig. 13 (c).

Figure 14 shows the comparison of deformation angle δ and weld bead geometry between 50 μm and 20 μm specimen thickness. It can be noticed here that even in the same aspect ratio of weld bead geometry, the deformation characteristics were different by the specimen thickness. Therefore, it was clarified that the welding deformation was influenced not only by the weld bead geometry but also by the thickness of specimen. It is important to understand the balance of stress with the relationship between the weld bead geometry and specimen thickness, and the further study of these relationships should be investigated in order to clarify the thermal deformation mechanism for micro-welding of thin sheet.

Conclusions

Main conclusions obtained in this study are as follows:

1. The specimen firstly deformed downward in the same direction of laser irradiation, and then deformed largely in the reversed direction after laser scanning due to the large shrinkage in the perpendicular to scanning direction.
2. Not only the weld bead geometry but also the specimen thickness has a great influence on the final deformation for thin sheet.
3. The extreme small distortion could be achieved by the proper weld bead geometry in micro-welding of thin sheet under the bead-on-plate welding condition.

References

[1] Schlueter, H., 2007. Laser Beam Welding, Welding Journal, 86 5, pp. 37-39.
[2] Tsukamoto, S., 2003. Laser Welding, Welding International, 17 10, pp. 767-774.
[3] Radaj, D., 1992. Heat Effects of Welding, Springer-Verlag, pp. 1, 9-11, 14, 149.
[4] Deng, D., Murakawa, H., 2008. Prediction of Welding Distortion and Residual Stress in a Thin Plate Butt-welded Joint, Computational Materials Science, 43, pp. 353-365.
[5] F. Vollertsen et al., 2005. Proceeding of the IWOTE'05: 1st International Workshop on Thermal Forming, 26, pp. 1-19
[6] Japan Stainless Steel Association, 2002. Stainless Steel Databook, The Nikkan Kogyo Shimbun (in Japanese), p. 209.
[7] Katayama, T., 1998. Three-dimensional Thermal Elastic-plastic Analysis of Laser Forming Process by Finite Element Method, Master Dissertation, Chubu University (in Japanese), pp. 34-35.
[8] Kazemi, K., Goldak, J. A., 2009. Numerical Simulation of Laser Full Penetration Welding, Computational Materials Science, 44, pp. 841-849.